Monitoring River Flow Status Using Low-Cost Wildlife Camera and Image Segmentation Artificial Intelligence

Jie Bao, Yunxiang Chen, Lupita Renteria, Morgan Barnes, Brieanne Forbes, Sophia McKever, Amy Goldman, Timothy Scheibe, James Stegen

Pacific Northwest National Laboratory, Richland, WA, 99352, USA

Abstract

Continuous measurement and monitoring of river or creek surface water coverage is crucial for studying the exchange fluxes between the surface and subsurface water. These fluxes directly impact carbon and nitrogen exchange and cycles, which are related to organic matter transport and reactions. While satellite and related techniques have been widely used for large-scale monitoring, they may not be accurate, sensitive, or cost-efficient for monitoring and tracking of surface water at fine-scale spatial (i.e., sub-meter) and temporal (i.e., daily) variations. This is especially true for small creeks with large plant canopy coverage. On-site in-situ sensors monitoring methods primarily yield point data, often insufficient in capturing the entire spatial distribution. Wildlife cameras have proven a cost-efficient way to continuously monitor surface water coverage of rivers and creeks. To efficiently analyze the images and/or videos from the wildlife cameras, in this study, two machine learning approaches, YOLOv8 and Mask2Former, have been applied. Both models were trained by images obtained from the public dataset ADE20k along with a small dataset from wildlife camera photos collected at the current study area. Once surface water coverage is segmented, the width of the surface water in real world can be approximated according to the wildlife camera, lens, and positioning parameters. In this

study, surface water was detected and monitored by applying the proposed approaches for the six wildlife cameras in the Yakima River Basin in 2023 to 2024 in United States of America. Though Mask2Former model provides slightly better transferability, both models can accurately capture the surface water from the wildlife cameras, which are installed in significantly different environments, such as the different brightness, contrast, and varying front scene object blockages. The proposed approach enables long-term continuous monitoring and quantification of river intermittency and water availability with high accuracy and low-cost, which will benefit river ecosystem research and management.

1. Introduction

River networks act as conduits between terrestrial and aquatic environments, mediating important biochemical processes that regulate the transport and fate of carbon and other nutrients (Battin, Kaplan et al. 2008). Research in stream metabolism, gas exchange, and sediment dynamics, repeatedly demonstrate how river networks are a critical component of biogeochemical cycles (Wohl, Hall et al. 2017) in space and time (Fisher, Brimm et al. 1998, Schlesinger and Bernhardt 2020).

The relevance and widespread occurrence of non-perennial streams have garnered rising interest in recent years. Non-perennial streams, which flow intermittently or episodically, are prevalent worldwide and constitute greater than 50% of global river networks (Snelder, Datry et al. 2013, Datry, Larned et al. 2014). Their unique hydrological, biological, and geochemical characteristics play critical roles in ecosystem functions, providing distinctive habitats and influencing biogeochemical processes such as nutrient cycling and organic matter

decomposition. However, non-perennial streams have been historically understudied, though the pioneering works were reported around 1960s to 1970s (Larimore, Childers et al. 1959, Clifford 1966, Williams and Hynes 1976). Recent research highlights their substantial contribution to hydrological and biogeochemical connectivity, emphasizing the urgency for their preservation and further study in order to predict and manage the impacts of climate change and human activities on water resources (Larned, Datry et al. 2010).

Monitoring non-perennial stream hydrodynamics presents a significant challenge due to their spatiotemporal variability. A straightforward approach is deploying sensors in the stream to monitor the water/no-water condition and/or the flow rate of the stream (Assendelft and Meerveld 2019). These in-situ monitoring methods primarily yield point data, often insufficient in capturing the entire spatial distribution of surface water within a stream.

In contrast, satellite remote sensing techniques offer broader spatial coverage and continuity, but they come with limitations, such as the spatial resolution, revisit frequency, and penetration. High-resolution satellite remote sensing images, whose space resolution reaches 0.15 m, are available for commercial use (MAXAR 2020), but their use for continuous monitoring over long time periods is limited by high costs. Therefore, more affordable and accessible multispectral images with systematic global coverage is usually at space resolution around 10 to 20 m, and the revisiting frequency around 5 to 10 days (Cavallo, Papa et al. 2022, Sentinel 2024). Therefore, the generally affordable satellite remote sensing is currently better suited for streams larger than 10 meters, because smaller, including intermittent, streams require high resolution images. Additionally, the plant and forest canopies may also a challenge for satellite remote sensing technique to stably visualize the stream surface water (Smith 1997, Hugue, Lapointe et al. 2016, Tomsett and Leyland 2019).

Besides the satellite remote sensing approach, on-site optical camera-based remote monitoring methods have been widely used to study water resources, such as large-scale particle image velocimetry (LSPIV) (Tauro, Olivieri et al. 2016, Zhen, Yang et al. 2017, Ghaffarian, Piegay et al. 2020) and stage-camera systems (Noto, Tauro et al. 2022, Tauro, Noto et al. 2022, Spasiano, Grimaldi et al. 2023). LSPIV can compute the stream velocity according to the video of the water surface pattern. Because it needs continuous video data, it is usually used in areas with long-term power supply or requires frequent visits to collect short term (less than one day) data over long timeframes. In contrast, stage-camera is a low-cost monitoring system for small streams and can work long-term off-grid. It uses a camera to record photos of the water surface with a reference scale in the water, which are used to back calculate the water surface elevation with a post-processing algorithm. Because the cameras have to be placed close to the reference scale, it is usually applied at small ephemeral streams (Noto, Tauro et al. 2022). Therefore, for the non-perennial streams with relatively large width varying, like between wider than 10 meters to near 0 meter, the stage-camera system may not get the representative wet fraction and width information of the stream.

Wildlife cameras, also known as trail cameras or game cameras, are typically used to observe animals in their natural habitats (Kemp, yarchuk et al. 2022). However, they have also found as a low-cost monitoring approach of water resources for scientific research, safety, and recreation activities (CreekVT 2024, NOC 2024, USGS 2024), due to its durability in outdoor conditions and fewer maintenance requirements with long-term use. Generally, wildlife cameras provide a view, which can be stored as time series photos and videos, of water surface and/or landscape of interests, so it is adaptable to various stream categories from small ephemeral streams to large perennial rivers. However, the photos and videos recorded by wildlife cameras cannot provide

quantitative measurements of the targeted stream directly. Traditionally it requires manual marking of the water boundaries on the photos for further analysis, making it too time consuming to be practical for long-term river water monitoring.

In this study, we developed a framework to monitor surficial river width and wet fraction using wildlife cameras in diverse river networks. The framework includes camera deployment instructions, a maintenance protocol, and machine learning models that can efficiently segment the stream water surface from the background of photos. Two machine learning models were investigated for the task of water surface recognition and separation. One is the convolutional neural network-based model YOLOv8 (Ultralytics 2023), and another model is the vision transformer-based model Mask2Former (Facebook 2022). The detailed introduction about the models and the training, validation, and testing are introduced in Section 2.2 and 3.1. Though Mask2Former model provides slightly better transferability, both models can accurately track the stream width and wet fraction, except several extreme weather and lighting conditions discussed in Section 3.2.

2. Methodology

2.1. Study domain and installation of wildlife cameras

Our 6 study sites are within the Satus Creek watershed, which is a 1114 km^2 watershed in the Yakama Nation Reservation in south-central Washington state, Untied States of America (Mundorff, Nish et al. 1977, Gellenbeck 1999). It spans from the Toppenish ridge in the north down to Horse Heaven Hills in the south (Mundorff, Nish et al. 1977). The area is mostly underdeveloped and is encompassed mostly by shrub-steppe vegetation, but also has some regions of coniferous forest and irrigated agriculture (Gellenbeck 1999). The Satus Creek

Watershed also accounts for nearly 10% of the Yakima river subbasin (NOAA 2020). The average precipitation ranges from 35 inches in the west to 10 inches in the east, of which is mostly snow (Mundorff, Nish et al. 1977). Sites (S30R, S31, S32, S38, S63, and S63P) were chosen to represent the watershed, including both perennial and non-perennial locations, and we have previously collected hydrobiogeochemical data (Fulton, Barnes et al. 2022, Grieger, Barnes et al. 2022, Delgado, Barnes et al. 2023, Kaufman, Delgado et al. 2023). For simple and short in this study, we call these deployed cameras as Yakima River Basin (YRB) cameras. The representative view of the six sites and the locations with corresponding latitude and longitude are show in Figure 1.

Figure 1: Locations and representative photos of the wildlife cameras deployed at six sites.

Depending on cellular service, we either deployed a cellular capable camera (SPYPOINT FLEX) or a non-cellular camera (CAMPARK TC08-4K). Only one camera was deployed per site. Both cameras cost between $100-200, and are widely available on various local or on-line stores. The SPYPOINT FLEX's cellular connection capability provides the convenience of accessing the photos and camera settings remotely, deployed at sites S38 and S63P, which can help on checking the status of cameras without visiting the sites after the first-time deployment. However, due to the cellular connection downloading speed limitation and only low-resolution images (highly compressed 720P image) downloadable through cellular connection, it is highly recommended to copy the raw high-resolution photos from the SD card directly during routine on-site work, if there are too many photos, like more than a hundred. The CAMPARK TC08-4K cameras were deployed at the locations without cellular service. Similarly, though CAMPARK TC08-4K camera can be accessed through Wi-Fi and Bluetooth connection remotely in a short distance range, it is still highly recommended to copy the raw high-resolution photos from the SD card directly during routine on-site work.

To deploy each of the cameras, we first selected a location along the river edge that had a clear view of the channel from bank to bank, and then pointed and positioned the lens towards the water. The camera was mounted on either a tree trunk, tripod, or attached to a tripod then attached to a tree trunk depending on the site, vegetation, and view. They were attached using a strap and secured with a locked wire rope. It was critical to make sure the camera was easily accessible, but outside of the public's view. The cameras were set to a timelapse mode and programmed to take pictures every 4 hours. A reference photo was taken at each camera during the initial deployment which had a measuring tape displaying 1 m in length, and the distance from the camera view was recorded. Various metadata were taken related to the location and tilt

of the camera, the surrounding environment, and some characteristics of the river. Every two weeks, pictures were directly downloaded from each SD card, each SD card was reformatted by using the reformat settings on the camera, and new metadata was recorded.

2.2. Image segmentation models and training dataset for wildlife camera photo

For measuring and monitoring the stream water surface, image segmentation machine learning models are needed to extract the stream water surface from the background on the wildlife camera photos. Image segmentation involves partitioning an image into multiple segments or 'pixels' which share similar attributes, and grouping these pixels together to form a more comprehensive understanding of the image. This plays a vital role in enriching object detection as it allows the model to differentiate individual objects in an image, even if they belong to the same category or are closely grouped. In this study, two state-of-the-art machine learning image segmentation models are used.

The first model is YOLOv8, which stands for "You Only Look Once version 8" (Redmon, Divvala et al. 2016). It is the eighth major iteration of an object detection system that is widely recognized for its superior effectiveness and efficiency. The model was developed and open-source released by Ultralytics (Ultralytics 2023). The primary goal of YOLOv8, is to precisely identify and localize objects in images and videos in real time. Generally, YOLOv8 is constructed by a series of convolutional layers (Zhang, Itoh et al. 1990), modified bottleneck cross stage partial network layers (Wang, Liao et al. 2020), a spatial pyramid pooling-faster layer (He, Zhang et al. 2015), concatenate layers, and up-sampling layers (PyTorch 2024). Because the training and inference speed is not the main concern in this study, the largest model (YOLOv8x-

seg) was used, which includes about 344.1 million trainable parameters in the whole neural networks.

The second model is Mask2Former, which is an innovative architecture designed for universal image segmentation (Facebook 2022). Different from the series of convolutional layers in YOLOv8 model, Mask2Former is based on the vision transformer model (Vaswani, Shazeer et al. 2017, Dosovitskiy, Beyer et al. 2020) which employs masked attention to extract localized features by constraining cross-attention within predicted mask regions (Chen, Schwing et al. 2021, Chen, Misra et al. 2022). This mechanism allows the model to focus on relevant areas, enhancing segmentation accuracy. In this study, the large size shifted window (Swin-L) transformer architecture (Liu, Lin et al. 2021) is used as the backbone in the Mask2Former model, and the model contains about 200 million trainable parameters.

For both models, the inputs of the model are the photos, and the outputs are the mask map of the detected objects and the corresponding class of the objects. There are two categories of labeled dataset used as training datasets in this study. One is the ADE20K public dataset (ADE20K 2017, Zhou, Zhao et al. 2017, Zhou, Zhao et al. 2018). There are totally 25,574 general photos with 150 labeled classes, which includes the most common objects in scenes of daily life, in ADE20K dataset. We subset these photos to include only natural landscapes for training and validation. Besides that, only the labeled objects that are related to natural surface waters were kept in the training, which included classes “sea”, “river”, “water”, “lake,” “whitewater”, and “wave”. These listed classes were merged into one class named as “surface water”. All the other irrelevant labels were removed from the training dataset. With such pre-treatment on the ADE20K dataset, there were a total of 1312 photos with 1437 labeled natural surface waters in the training dataset, and 59 photos with 65 labeled natural surface water in the validation dataset.

In this manuscript, we call this dataset as ADE20K for short, though it is just a subset of ADE20K dataset. The second category of labeled dataset is directly from the YRB wildlife cameras' photos. 304 photos were selected from all the YRB wildlife camera photos with 1546 natural surface water labels. 76 photos were selected with 361 labeled natural surface water for validation.

Additionally, there are two categories of labeled dataset were used as testing dataset for benchmarking accuracy of trained models. One is the YRB wildlife cameras' photos. There are 24 photos with 104 labeled natural surface water patches. These 24 photos are not in either training or validation dataset. The second category of testing dataset is from wildlife camera photo available on creekvt.com (CreekVT 2024), which are monitoring the creeks in the state Vermont United States of America for identifying whether the stream condition safe for kayakers. 12 photos are selected with 19 labeled natural surface water patches. Figure 2 shows the example photos from ADE20K, YRB wildlife cameras, and CreekVT wildlife cameras for the training, validation, and testing in this study. The sources of the images, the number of the images and labels are summarized in Table 1.

(a) (b) (c)

Figure 2: Example of the labeled photos. (a) ADE20K dataset; (b) YRB wildlife cameras' photo; (c) CreekVT wildlife cameras' photo.

Table 1: Summary of dataset used in this study.

Source of the images	ADE20K	YRB cameras	CreekVT
Training (Num. of images/Num. of labels)	1312/1437	304/1546	NA
Validation (Num. of images/Num. of labels)	59/65	76/361	NA
Testing (Num. of images/Num. of labels)	NA	24/104	12/19

2.3. Post-processing to the real dimensions with cameras' metadata

For accurate conversion from photo to real-world dimensions, a widely applied rectifying algorithm is using at least 6 ground control points (GCP), with known real-world coordinates, to calibrate all the parameters in the rectifying algorithm (Mikhail and Ackermann 1976, Fujita, Muste et al. 1998, Muste, Fujita et al. 2008). However, in this study, no GCP has been used on-site, so a relatively simple algorithm was used to approximate the real-word dimensions, according to the metadata of the cameras, including the camera height above the water surface, camera tilt angle, the camera senser size, and camera focal length. The actual distance (D) between the camera and the object on the photo is estimated by

$$D = \tan(\beta)\, H\,, \tag{1}$$

where H is the camera height above the water surface. $\beta = \frac{\pi}{2} - \tau - \alpha$, where τ is the camera tilt angle, as shown in Figure 3(a), and $\alpha = \text{atan}\,(\frac{h}{f})$. h is the distance between the object and center line on the camera sensor, as shown in Figure 3(b) (dark blue: river, green: ground, light blue: sky), and f is the focal length of camera lens. The actual width (W) of the water surface is estimated by

$$W = \frac{\omega H \cos(\alpha)}{f \cos(\beta)}\,, \tag{2}$$

where ω is the width of the water surface on the camera sensor. The value of h and ω are estimated according to the relative position on the photo and the sensor size, which are 4.22 × 2.38 mm in this study.

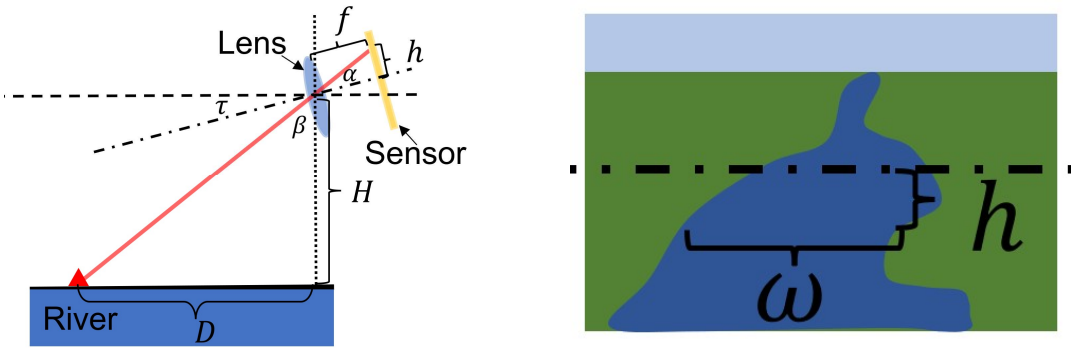

(a) (b)

Figure 3: Sketch of the method for approximate the actual distance and width of the water surface according to the wildlife camera photos. (a) Sketch of the camera's parameters used for estimation; (b) Sketch of the image on the camera sensor for estimation.

The examples of the estimated water surface width maps on wildlife camera's photos are shown in Figure 4. The comparisons between the photo-based stream width approximation and the on-site measurements are shown and discussed in Section 3.2. Please note that there are several issues in the Equation (2) would cause uncertainty on stream width approximation. The camera height above the water (H) is not a constant value in real-world, because surface water elevation varies with time, while camera is usually installed at a fixed height above ground. Additionally, Eq. (2) also assume the water surface is perfect horizontal, but the practical stream water surface usually has elevation gradient.

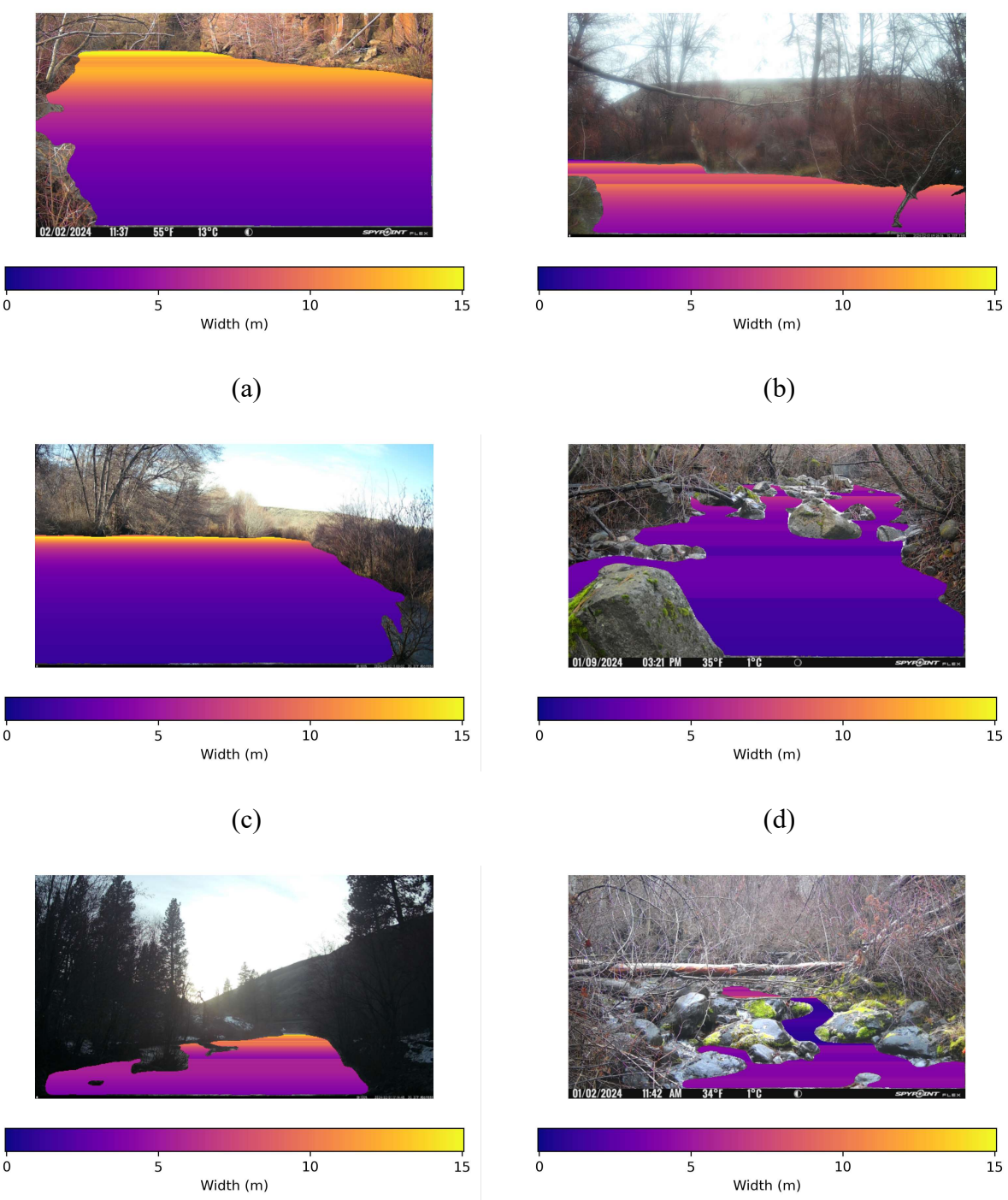

Figure 4: Example width map of the surface water for the six sites. (a) S30R; (b) S31; (c) S32; (d) S38; (e) S63; (f) S63P.

3. Results

3.1. Model accuracy

Both YOLOv8 and Mask2Former models were trained on the two training datasets (ADE20K and YRB wildlife cameras) separately, so there are four trained models: YOLOv8 trained by ADE20K nature landscape photos, Mask2Former trained by ADE20K nature landscape photos, YOLOv8 trained by YRB wildlife camera photos, and Mask2Former trained by YRB wildlife camera photos. For short, they are named as YOLOv8-ADE20K, Mask2Former-ADE20K, YOLOv8-YRB, and Mask2Former-YRB respectively as listed in Table 2. The model was trained on one Nvidia A100 80G GPU. The four trained models were evaluated by the two testing datasets (YRB and CreekVT wildlife camera). The example of the model predicted masks for the segmented surface water comparing with the ground truth are listed in Figure 5. The identified water surfaces are marked by the semi-transparent red mask in Figure 5. The evaluation of the accuracy of the models are listed in Table 2. The average precision (AP) is used as the metrics of quantifying model accuracy. The AP50 represent the average precision calculated at an IoU (intersection over union) threshold of 0.5. In other words, it only counts detections as true positives if they have IoU of 50% or more with the ground truth. Similarly, AP75 only counts detections as true positives if they have IoU of 75% or more. AP, in the table, represent the average from AP50 to AP95 with increased interval of IoU of 5%.

It is obvious that the modeled trained by ADE20K dataset cannot capture the stream surface accurately, especially for the sites S32, S38, S63, and S63P, because the boundary of the stream water surface is very complex, which are not common in the general landscaping photos in public dataset ADE20K. The models trained with YRB wildlife camera photos can provide much better inference accuracy. The YOLOv8-YRB model has AP at 39% for the YRB test dataset, which is better than Mask2Former's accuracy 31%. For the test dataset from CreekVT, the

model YOLOv8-YRB model's accuracy decrease obviously to AP=31%. In contrast, Mask2Former-YRB model's accuracy increased to AP=41% for the CreekVT data. The potential reason is the complex stream surface boundary in YRB wildlife camera photos. YOLOv8 focuses on the details of the small patches of water surface and their complex boundaries, but loses partial of the feature capturing accuracy of general water surface. While Mask2Former-YRB keeps accuracy on capture features of the general understanding of water surface, by partially sacrificing the accuracy on tracking the small patches of water and their complex boundaries. This makes Mask2Former-YRB provide more reliably monitoring results when applied it to different camera photos that are from various locations.

Camera ID	Ground truth	YOLOv8-ADE20K	Mask2Former-ADE20K	YOLOv8-YRB	Mask2Former-YRB
S30R					
S31					
S32					
S38	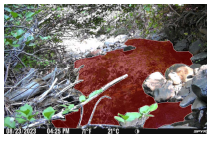				
S63					

Figure 5: Examples of the model prediction on the test dataset comparing to the ground truth.

Table 2: Model accuracy on the two test datasets: YRB wildlife camera dataset and CreekVT dataset.

	YOLOv8-ADE20K			Mask2Former-ADE20K			YOLOv8-YRB			Mask2Former-YRB		
	AP	AP50	AP75	AP	AP50	AP75	AP	AP50	AP75	AP	AP50	AP75
YRB wildlife camera test dataset	5.2	10.1	6.6	5.4	15.6	1.9	39.1	71.0	41.4	29.9	55.5	25.4
CreekVT test dataset	16.2	50.8	5.7	14.4	39.1	15.1	30.9	56.3	24.9	41.0	57.0	52.5

3.2. Steam width variation with time for the 6 cameras

As discussed in Section 3.1, the model trained by ADE20K dataset cannot provide accurate and reliable segmentation on water surface, so only the models trained by YRB wildlife camera photos (YOLOv8-YRB, Mask2Former-YRB) are used to inference the time series photos for the six sites. The cameras were set to take photo every 4 hours, so there are large number of photos in night vision mode. Such photos are very dark, and extremely difficult to recognize the objects,

so only the photos taken during day light conditions are used for stream surface segmentation and evaluations.

The wet fraction variations and the estimated width for the six investigated sites are shown in Figure 6. Because the cameras were not installed at the same time, the start dates of the data in Figure 6 are not the same for the six sites. The wet fraction is defined as the actual wetted area normalized by the possible maximum wetted area of the stream water surface, so it is unitless value. The rocks and/or small islands that are out of the water surface are deducted from the calculation of wetted area, so the wet fraction calculation deducts the dry areas in the middle of the stream. The width is the distance between the two shorelines of the stream as introduced in Section 2.3, so the small dry islands and/or the rocks out of the water surface does not impact the measurements of the width. There are several data gap in Figure 6. This is caused by the cameras not taking any day light condition photos during these gap time periods, due to the camera's settings error. Additionally, as stated in Section 2.3, the algorithm from photo to real-world dimensions was a simplified approximation approach when no on-site GPC data available, so it is possibly less reliable than wet fraction data, which does not need any addition conversion algorithm. The on-site measured stream widths are also shown in Figure 6. Generally, the estimated width of the water surface match the on-site measurements fairly well. Please note that the on-site measurements were the distance between two arbitrarily selected points at the two sides of the stream, which are not exactly the surface water edge-to-edge distance and may include the partially wet riverbank and riverbed. It is not the averaged width of the stream surface in the view of the wildlife camera, and the on-site measurements at different time may from different measuring points. Therefore, the on-site measurements are only for providing references of the scale of the investigated streams, like sub meter small creek, 5-meter level, 10-

meter level, above 20-meter level, and so on, so it is not expected to provide actual time varying width information.

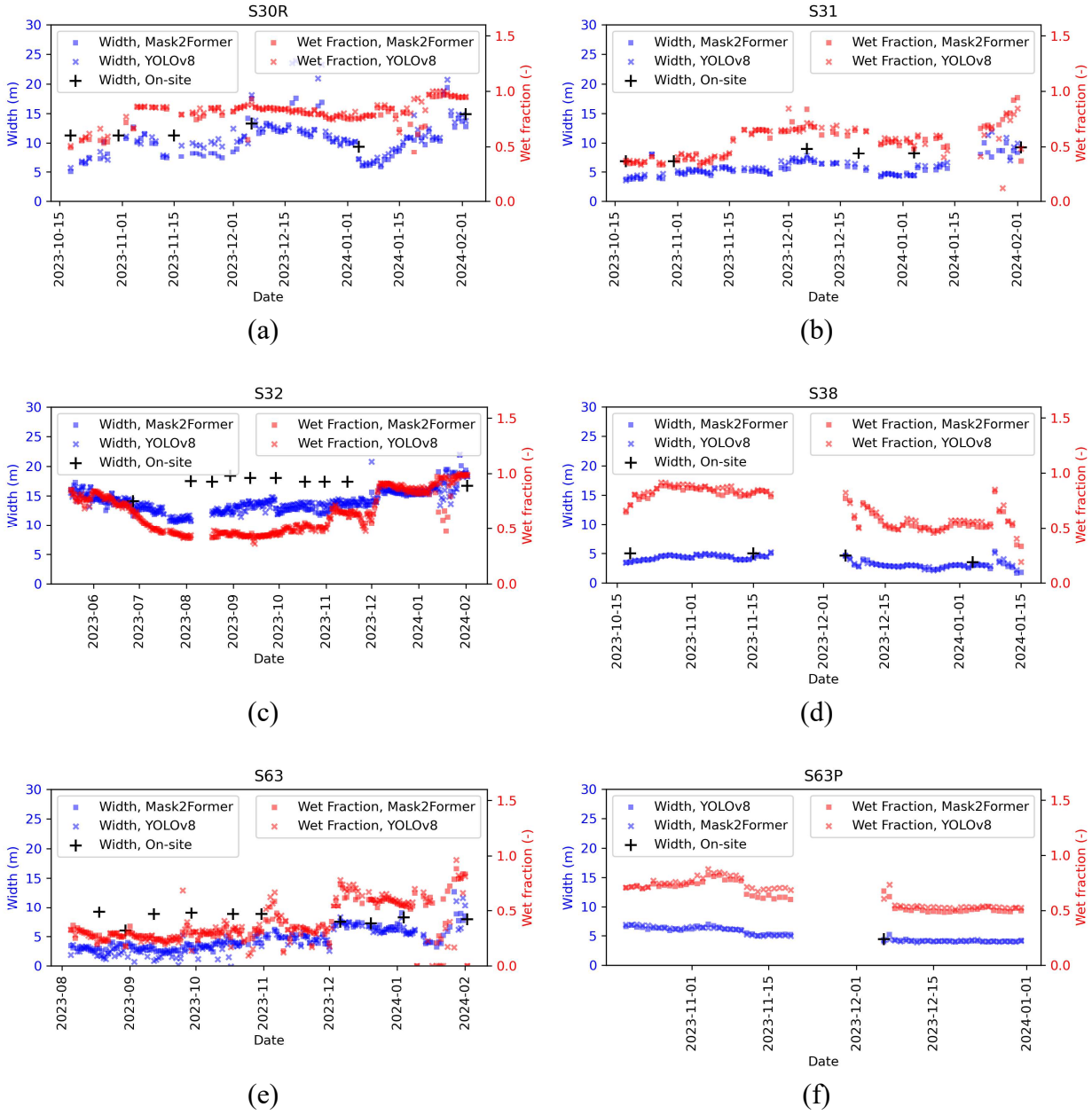

Figure 6: Stream wet fraction and width time series for the investigated six sites. (a) S30R; (b) S31; (c) S32; (d) S38; (e) S63; (f) S63P.

Generally, both YOLOv8 and Mask2Former models provide similar long-term wet fraction variation for the six sites. However, the wet fraction estimated based on YOLOv8 inference shows slightly higher short-term fluctuation than the ones from Mask2Former, especially for sites S30R, S31, and S63. The stream water surface usually does not dramatically change in a short duration, such as one or two days. These higher fluctuations are caused by the stability and transferability of the image segmentation models. The accuracy comparison in Table 2 shows that Mask2Former provide higher stability and transferability then YOLOv8 when processing the photos, that the contents in it are quite different from the training dataset. In all the photo series for inference, there are many photos with different light conditions that are not available in the training dataset, though the landscaping scene are the same. For example, variability in sunlight may cause lens flare, over exposure, and sometimes loss of necessary details in the shadow regions. An example comparison between the two models' inference in an extreme lighting condition for site S63 is shown in Figure 7(a) for YOLOv8-YRB and (b) Mask2Former-YRB. The photo was taken on October 28th, 2023, 3:15PM PST during sunset at site S63. It is obvious that YOLOv8 model does not detect the water surface in red circle, neither the rocks in yellow circle, while Mask2Former provides much better results. In such or similar situation, Mask2Former's inference is more stable that YOLOv8, and then slightly lower short-term fluctuations on stream surface water wet fractions.

Additionally, frozen surface water and snow also cause uncertainty on the inference of water surface from the two models. An example comparison for the frozen surface water covered by snow is shown in Figure 8(a) for YOLOv8-YRB and (b) Mask2Former-YRB. The photo was taken on January 19th, 2024, 5:00PM PST at site S32. It is challenging to differentiate whether the surface below the snow is frozen stream or the terrestrial landscape without seeing the photos

taken in warmer conditions. YOLOv8-YRB model simply considers the large flat surface as stream water surface, while Maks2Former-YRB model does not treat it as surface water. In such situations, the wet fraction estimated from Mask2Former-YRB model shown in Figure 6(c) provide very large fluctuation from January 17th 2024 to January 22nd 2024. It is possible that adding a few such photos with labeled snow surface as water surface may reduce the uncertainty on the inference. However, it is not recommended due to potential model stability and transferability issues. Labeling some object that is obviously not visually belonging to the object class may significantly confuse the model and would be harmful to the overall model accuracy. Therefore, the wildlife camera-based stream surface monitoring is only recommended for areas that do not continuously have frozen surface water and snow. For example, the frozen time should no longer than 20% of the total monitoring time.

(a) (b)

Figure 7: Comparison between the two models' inference in an extreme lighting condition for site S63. (a) YOLOv8-YRB; (b) Mask2Former-YRB.

(a) (b)

Figure 8: Comparison between the two models' inference for frozen stream water surface covered by snow for site S32. (a) YOLOv8-YRB; (b) Mask2Former-YRB.

Besides the scenarios mentioned above, there are several conditions that are difficult for image segmentation models to handle, such as night vision mode and mist as the example photos shown in Figure 9(a) and (b) respectively. Therefore, the wildlife camera photos cannot be used to monitor water coverage changes within one day for the purpose of comparing the variation between day and nighttime. The mist and/or rain is usually not a major issue, because it should not last very long. The mist on lens usually disappear after a sunny day without needs of in-person maintenance. Missing a few days tracking information is acceptable for the long-term monitoring. If the length of nighttime and the length of mist or raining time is main concern in the area of investigation, the proposed wildlife camera photo with machine learning water surface separation may not be an appropriate approach.

(a) (b)

Figure 9: Examples of the photos that are difficult for image segmentation model. (a) night vision mode photo; (b) photo in mist or rain.

4. Conclusion and discussion

Both YOLOv8 and Mask2Form image segmentation models were tested in this study to separate the stream water surface from the wildlife camera photos for monitoring the wet fraction variation at six sites in Status creek watershed in Yakima River Basin. It is demonstrated that, the models trained by the general public photo dataset ADE20K are not accurate enough for the task of wildlife camera photos recognition. It is very necessary to use the actual wildlife camera photos to train the models to enhance accuracy of the surface water segmentation. With a total of 380 labeled wildlife camera photos used as training and validation datasets, accuracy of both models significantly increased. The Mask2Former-YRB model showed better stability and transferability for the different landscaping scene and extreme lighting conditions compared to the YOLOv8 model. As shown in Table 2, for the photos from CreekVT, which is completely not used in model training and validation, Mask2Former-YRB model still achieve average precision 41%, while YOLOv8-YRB only has 31%. Overall, Mask2Former-YRB provided more reliable monitoring results as discussed in Section 3.2 and compared in Figure 7. This means that

for new installed cameras in the future, Mask2Former-YRB model can directly be used for the segmentation task without retraining, while YOLOv8-YRB model would need adding new cameras' photo to the training dataset for retraining.

As demonstrated in this study, wildlife cameras are a cost-efficient way to continuously monitor the river or creek surface water, and machine learning models can provide efficient and accurate estimation of variable wet fractions, although there are still several scenarios where this application is limited. The first situation is the frozen water surface covered by snow as discussed in Section 3.2 and shown in Figure 8. Without collecting photos taken during warmer time points, it is hard to justify whether the surface below the snow is frozen stream or other possible flat surface such as land or dry riverbed. Therefore, the proposed approach is not recommended for the areas that continuously have frozen and/or snow weather conditions. For example, the frozen time should be no longer than 20% of the total monitoring time. In addition, it is almost impossible to separate the water surface from the terrestrial landscape with night vision mode photos as shown in Figure 9(a). The third situation is mist and rain as shown in Figure 9(b). In such weather conditions, the photo can be very blurred, making the model unable to differentiate the surface water during the segmentation step.

The proposed framework of wildlife camera with AI image segmentation provides a cost-efficient monitoring system for both small perennial and non-perennial. For large perennial stream, though the proposed framework technically is also capable, satellite based remote sensing would be a more efficient approach. The proposed framework works completely off-grid, and can be applied in many environments and locations. It can adapt to monitoring large variations in stream width from over 10 meters to near zero. It can work continuously for a few months without any on-site maintenance, and still can provide sub-daily temporal resolution. The

proposed AI model also provides the flexibility of measuring the stream width with or without deduction of the dry island or rocks in the middle of the surface water.

5. Acknowledgement

We thank the Confederated Tribes and Bands of the Yakama Nation Tribal Council and Yakama Nation Fisheries for working with us to facilitate sample collection and optimization of data usage according to their values and worldview. Research performed through PNNL's River Corridor Scientific Focus Area (SFA) project, supported by the United States Department of Energy (DOE) Office of Biological and Environmental Research (BER), Environmental System Science program (ESS).

6. Data availability

The source images are available at ESS-DIVE at https://data.ess-dive.lbl.gov/datasets/doi:10.15485/2319247 (Renteria, Bao et al. 2024).

Reference

ADE20K (2017). https://groups.csail.mit.edu/vision/datasets/ADE20K/.

Assendelft, R. S. and H. J. I. v. Meerveld (2019). "A Low-Cost, Multi-Sensor System to Monitor Temporary Stream Dynamics in Mountainous Headwater Catchments." Sensors **19**: 4645.

Battin, T. J., et al. (2008). "Biophysical controls on organic carbon fluxes in fluvial networks." Nature Geoscience **1**: 95-100.

Cavallo, C., et al. (2022). "Exploiting Sentinel-2 dataset to assess fow intermittency in non-perennial rivers." Scientifc Reports **12**: 21756.

Chen, B., et al. (2022). "Masked-attention Mask Transformer for Universal Image Segmentation." CVPR.

Chen, B., et al. (2021). "Per-Pixel Classification is Not All You Need for Semantic Segmentation." NeurIPS.

Clifford, H. F. (1966). "The ecology of invertebrates in an intermittent stream." Investigations of Indiana Lakes and Streams **7**: 57-98.

CreekVT (2024). "CreekVT." from https://creekvt.com/.

Datry, T., et al. (2014). "Intermittent Rivers: A Challenge for Freshwater Ecology." BioScience **64**(3): 229-235.

Delgado, D., et al. (2023). Spatial Study 2022: Surface Water Samples, Cotton Strip Degradation, and Hydrologic Sensor Data across the Yakima River Basin, Washington, USA (v2). ESS-DIVE.

Dosovitskiy, A., et al. (2020). "An Image is Worth 16x16 Words: Transformers for Image Recognition at Scale." arXiv.

Facebook (2022). "Mask2Former." from https://github.com/facebookresearch/Mask2Former.

Fisher, S. G., et al. (1998). "Material Spiraling in Stream Corridors: A Telescoping Ecosystem Model." Ecosystems **1**: 19-34.

Fujita, I., et al. (1998). "Large-scale particle image velocimetry for flow analysis in hydraulic engineering applications." Journal of Hydraulic Research **36**: 397-414.

Fulton, S. G., et al. (2022). Spatial Study 2021: Sensor-Based Time Series of Surface Water Temperature, Specific Conductance, Total Dissolved Solids, Turbidity, pH, and Dissolved Oxygen from across Multiple Watersheds in the Yakima River Basin, Washington, USA (v2). ESS-DIVE.

Gellenbeck, K. (1999). A Spatial and Temporal Analysis of Riparian Vegetation along Satus Creek on the Yakama Indian Reservation. Resource Management. Central Washington University, Central Washington University. **Master**.

Ghaffarian, H., et al. (2020). "Video-monitoring of wood discharge: first inter-basin comparison and recommendations to install video cameras." earth Surface Processes and Landforms **45**(10): 2219-2234.

Grieger, S., et al. (2022). Spatial Study 2021: Sample-Based Surface Water Chemistry and Organic Matter Characterization across Watersheds in the Yakima River Basin, Washington, USA (v2). ESS-DIVE.

He, K., et al. (2015). "Spatial Pyramid Pooling in Deep Convolutional Networks for Visual Recognition." arXiv.

Hugue, F., et al. (2016). "Satellite-based remote sensing of running water habitats at large riverscape scales: Tools to analyze habitat heterogeneity for river ecosystem management." Geomorphology **253**: 353-369.

Kaufman, M. H., et al. (2023). Spatial Study 2022: Water Column, Sediment, and Total Ecosystem Respiration Rates across the Yakima River Basin, Washington, USA. ESS-DIVE.

Kemp, C., et al. (2022). "A Guide to Using Wildlife Cameras for Ecological Monitoring in a Community-based Context." from https://wildcams.ca/site/assets/files/1386/cbm_wildlife_camera_guide-_aug2022.pdf.

Larimore, R. W., et al. (1959). "Destruction and reestablishment of stream fish and invertebrates affected by drought." Transactions of the American Fisheries Society **88**: 261-285.

Larned, S. T., et al. (2010). "Emerging concepts in temporary-river ecology." Freshwater Biology **55**: 717-738.

Liu, Z., et al. (2021). "Swin Transformer: Hierarchical Vision Transformer using Shifted Windows." arXiv.

MAXAR (2020). "Introducing 15 cm HD: The Highest Clarity From Commercial Satellite Imagery." from https://blog.maxar.com/earth-intelligence/2020/introducing-15-cm-hd-the-highest-clarity-from-commercial-satellite-imagery.

Mikhail, E. M. and F. E. Ackermann (1976). Observations and least squares. New York, USA, IEP.

Mundorff, M. J., et al. (1977). Water resources of the Satus Creek Basin, Yakima Indian Reservation, Washington.

Muste, M., et al. (2008). "Large-scale particle image velocimetry for measurements in riverine environments." Water Resources Research **44**: W00D19.

NOAA (2020). "Satus Creek Watershed Restorat." from https://www.webapps.nwfsc.noaa.gov/apex/f?p=409:19:::::P19_PROJECTID:39159507.

NOC (2024). "Nantahala River Live Webcam." from https://noc.com/live-webcam/.

Noto, S., et al. (2022). "Low-cost stage-camera system for continuous water-level monitoring in ephemeral streams." Hydrological Sciences Journal **67**(9): 1439-1448.

PyTorch (2024). "Upsample." from https://pytorch.org/docs/stable/generated/torch.nn.Upsample.html.

Redmon, J., et al. (2016). You Only Look Once: Unified, Real-Time Object Detection. 2016 IEEE Conference on Computer vision and Pattern Recognition. Las Vegas, NV, USA.

Renteria, L., et al. (2024). Timeseries Photos and (Meta)Data of Variably Inundated Streams Across The Yakima River Basin, Washington, United States.

Schlesinger, W. H. and E. S. Bernhardt (2020). Biogeochemistry : an analysis of global change. London, Academic Press, an imprint of Elsevier.

Sentinel (2024). "Sentinel Online." from https://sentinels.copernicus.eu/web/sentinel/.

Smith, L. C. (1997). "Satellite remote sensing of river inundation area, stage, and discharge: a review." Hydrological Processes **11**: 1427-1439.

Snelder, T. H., et al. (2013). "Regionalization of patterns of flow intermittence from gauging station records." Hydrol. Earth Syst. Sci. **17**(7): 2685-2699.

Spasiano, A., et al. (2023). "Testing the theoretical principles of citizen science in monitoring stream water levels through photo-trap frames." Frontiers in Water **29**.

Tauro, F., et al. (2022). "Assessing the Optimal Stage-Cam Target for Continuous Water Level Monitoring in Ephemeral Streams: Experimental Evidence." Remote Sensing **14**(23): 6064.

Tauro, F., et al. (2016). "Flow monitoring with a camera: a case study on a flood event in the Tiber River." Environmental Monitoring and Assessment **188**(118).

Tomsett, C. and J. Leyland (2019). "Remote sensing of river corridors: A review of current trends and future directions." river Research and Applications **35**: 779-803.

Ultralytics (2023). "YOLOv8." from https://github.com/ultralytics/ultralytics.

USGS (2024). "California Water Science Center Webcams." from https://www.usgs.gov/centers/california-water-science-center/multimedia/webcams.

Vaswani, A., et al. (2017). "Attention Is All You Need." arXiv.

Wang, C. Y., et al. (2020). CSPNet: A New Backbone that can Enhance Learning Capability of CNN. Conference on Computer Vision and Pattern Recognition Workshops Seattle, WA, UDA.

Williams, D. D. and H. B. N. Hynes (1976). "The ecology of temporary streams I. The faunas of two Canadian streams. Internationale Revue der Gesamten." Hydrobiologie und Hydrographie **61**: 761-787.

Wohl, E., et al. (2017). "Carbon dynamics of river corridors and the effects of human alterations." Ecological Monographs **87**(3): 379-409.

Zhang, W., et al. (1990). "Parallel distributed processing model with local space-invariant interconnections and its optical architecture." Applied Optics **29**(32): 4790-4794.

Zhen, Z., et al. (2017). IP camera-based LSPIV system for on-line monitoring of river flow. 2017 13th IEEE International Conference on Electronic Measurement & Instruments (ICEMI), Yangzhou, China.

Zhou, B., et al. (2017). Scene Parsing through ADE20K Dataset. 2017 IEEE Conference on Computer Vision and Pattern Recognition, Honolulu, HI, USA.

Zhou, B., et al. (2018). "Semantic Understanding of Scenes through the ADE20K Dataset." arXiv.